Purely Optical, Reversible, Read-Write-Erase Cycling Using Photoswitchable Beads in Micropatterned Arrays

Heyou Zhang, Pankaj Dharpure, Michael Philipp, Paul Mulvaney, Mukundan Thelakkat, and Jürgen Köhler*

Using surface-templated electrophoretic deposition, arrays of polymer beads (photonic units) incorporating photo-switchable DAE molecules are created, which can be reversibly and individually switched between high and low emission states by direct photo-excitation, without any energy or electron transfer processes within the molecular system. The micropatterned array of these photonic units is spectroscopically characterized in detail and optimized with respect to both signal contrast and cross-talk. The optimum optical parameters including laser intensity, wavelength and duration of irradiation are elucidated and ideal conditions for creating reversible on/off cycles in a micropatterned array are determined. 500 such cycles are demonstrated with no obvious on/off contrast attenuation. The ability to process binary information is demonstrated by selectively writing information to the given photonic unit, reading the resultant emissive signal pattern and finally erasing the information again, which in turn demonstrates the possibility of continuous recording. This basic study paves the way for building complex circuits using spatially well-arranged photonic units.

H. Zhang, M. Philipp, J. Köhler
Spectroscopy of soft Matter
University of Bayreuth
95440 Bayreuth, Germany
E-mail: juergen.koehler@uni-bayreuth.de
P. Dharpure, M. Thelakkat
Applied Functional Materials
University of Bayreuth
95440 Bayreuth, Germany
P. Mulvaney
ARC Centre of Excellence in Exciton Science
School of Chemistry
University of Melbourne
Parkville, VIC 3010, Australia
M. Thelakkat, J. Köhler
Bavarian Polymer Institute
University of Bayreuth
95440 Bayreuth, Germany
M. Thelakkat, J. Köhler
Bayreuther Institut für Makromolekülforschung (BIMF)
95440 Bayreuth, Germany

1. Introduction

Electronic devices are one of the most important inventions of the last century and their impact on everyday life cannot be overestimated. These devices rely on integrated circuits that correspond to a network of interconnected logic gates. A logic gate generates a binary output "1" or "0" depending on the combination of input stimuli and runs on electrons as signal carriers. In contrast, an optical gate may be actuated with the input of light and allows one to exploit not only intensity (i.e., the number of photons per unit time) but also properties such as wavelength or polarization, thereby enabling opportunities for massive parallelization of data transfer. Hence, all-optical circuitry remains a long-cherished goal in the fields of high-density data storage and ultrafast communications. Accordingly, the transition from electrical to optical networks has attracted much attention.[1–4]

The challenge to develop devices for signal transduction that run on photons rather than on electrons is extremely demanding and requires materials that feature high photochemical/photophysical stability, high fatigue resistance, a rapid response, thermally irreversible bistability, and suitable experimental protocols for immobilizing the photon sources/sinks. All of these bottlenecks have thus far prevented the development of all-optical logic circuits. Photoswitchable molecules are a promising platform for meeting these requirements as they can be interconverted between two bistable, isomeric forms by absorption of light of two different wavelengths.[5–7] This offers the opportunity to optically encode information as the presence or absence of a specific isomer.[2,5,8–11] In the past, several strategies based on photochromism have been proposed to realize all-photonic logic functions for controlling energy and charge transfer efficiencies between photoswitches and dye molecules.[12–17] This has led to the idea of photonic logic gates.[18–24] However, for some of the demonstrated logic functions, the output of one gate corresponds to a change in absorbance at a certain wavelength,[19,21] while for others it is necessary to take a spectral scan[19] or even to perform a tedious principal component analysis to determine spectral changes.[22] To date no study has demonstrated an array of gates or controlled spatial immobilization of the photonic units in a solid-state device and, furthermore, none has shown that individual gates can be optically addressed. These are two of the

**ADVANCED
SCIENCE NEWS**

www.advancedsciencenews.com

**ADVANCED
OPTICAL
MATERIALS**

www.advopticalmat.de

key prerequisites that must be fulfilled in order to utilize these outputs to concatenate two or more logic gates.

Recently, Irie and coworkers introduced a new class of photochromic molecules based on dibenzothienylperfluorocyclopentenes that are intrinsically fluorescent on photocyclization, and which are therefore termed "turn-on" photoswitches.[25–29] Accordingly, irradiation with UV light leads to a ring cyclization reaction of the low emitting (LE) open-isomer, transforming it into a highly emitting form (HE) that can be probed with VIS light. Such turn-on photoswitches can be reversibly switched between LE and HE states. However, the light used for probing the emission can also induce the cycloreversion process, resulting in the LE form of the photoswitches. Both processes, i.e., emission of a photon and conversion of the switches to the LE form are in competition with each other and mutually exclusive. Such "turn-on" switches have been used to demonstrate high-security authentication of micrometre-sized optical patterns.[30] Unfortunately, one write-read cycle took several hours to complete. Nevertheless, these results offer micropatterning opportunities with photochromic molecules and are encouraging for the development of all-photonic gates. Ultimate miniaturization envisages the use of a single photochromic molecule for encoding one bit. However, as has been shown recently, individual molecules are generally not suited to encode unequivocal HE/LE states[31,32] due to the unavoidable blinking of single objects.[33–36] Yet, as suggested in[32] a small ensemble of photochromic molecules will be sufficient for an unambiguous discrimination of HE and LE levels.

Here we immobilize an ensemble of photoswitchable 1,2-Bis(2-ethyl-6-phenyl-1-benzothiophene-1,1-dioxide-3-yl)perfluorocyclopentene (abbreviated as DAE) "turn-on" photoswitches by incorporating these molecules into polystyrene beads. Then the dye-loaded beads can be actively micropatterned by surface templated electrophoretic deposition (STEPD) within seconds into predefined structures. This allows the fabrication of large-area arrangements of nanoparticles with high precision that can be considered as individual photonic units. In the following, it will be demonstrated that the DAE molecules embedded in polystyrene beads can be switched reversibly hundreds of times between HE and LE states without degradation, and that an array of such DAE-loaded PS beads is fully controllable using light as the external stimulus. The limiting conditions for photoaddressing individual photonic units to achieve i) maximum contrast between HE and LE states that can be associated with the binary outputs "1" and "0", ii) minimum cross-talk between adjacent photonic units, and iii) the feasibility of reversible read-write erase cycles will be systematically explored. By deliberately moving the array of beads relative to the focus of the UV illumination, information can be inscribed sequentially into a group of polymer beads, where each write–read–erase cycle takes just a few seconds. This study of well-structured and spatially immobilized DAE moieties elucidates the interplay of experimental parameters such as illumination intensities, wavelengths, and illumination times for optimum imprinting of information on microstructured matter with optical means and paves the road for the creation of more complex systems based on photonic logic gates.

2. Results

2.1. Photophysics of DAE Molecules

The DAE molecule undergoes reversible isomeric changes upon irradiation with light. Illumination in the UV spectral range (280–350 nm) induces a photocyclization reaction resulting in a highly emissive (HE) state, whereas illumination in the visible spectral range (420–520 nm) leads to a photo-cycloreversion reaction, which yields a low-emissive (LE) state, **Figure 1a** top. For immobilization, the photochromic DAE molecules were incorporated into polystyrene (PS) nanobeads with a diameter of ≈310 nm. Thereby, each individual bead accommodates ≈10^6 DAE molecules (see Supporting Information). In order to test whether the photophysical properties of the DAE molecules were conserved upon incorporation into the PS nanobeads, the UV/VIS spectra of DAE in toluene solution and embedded in PS in water were compared (for details see Supporting Information). As shown in Figure 1b, the emission spectra of DAE in solution and embedded in PS are in close agreement with each other both for the LE and the HE state. This allows clear discrimination between the two emission intensity levels in DAE-doped PS beads. It is worth noting that the LE emission shown in Figure 1b (blue lines) does not stem from the open-ring isomers but rather from the remaining fraction of closed-ring isomers due to an incomplete close-to-open transformation of the chromophores.[37]

2.2. Photoaddressing Micropatterned Arrays

Next, the dye-loaded beads were assembled into a 2D lattice combining electrophoretic deposition and electron beam lithography (EBL), referred to as surface-templated electrophoretic deposition (STEPD). With STEPD electrically charged nanoparticles can be positioned under the influence of an external electric field onto a predefined template that has been prepared with EBL, Figure 1c. This allows the creation of large-area assemblies of nanoparticles with high precision. A detailed description of the method is described elsewhere.[38] We used these techniques to position individual DAE-loaded PS beads into predefined cavities that were crafted by EBL to form a grid with 5 µm spacing, Figure 1d. Based on dynamic light scattering and zeta-potential measurements, the DAE-loaded PS bes feature a hydrodynamic size of 334 nm ± 20 nm and a zeta-potential of −33.9 mV ± 0.5 mV (see Supporting Information). Hence, the cavity size was fabricated to be 500 nm × 500 nm, and a positive potential (+4 V with respect to counter ITO) was applied during the STEPD assembly. The sample was attached to a piezo stage for precise movements of the array and the cell was mounted in a home-built, dual-light, microscope setup for switching and exciting single beads. The green circle in Figure 1d refers to the area of ≈70 µm in diameter that is illuminated with the VIS light, and the white square refers to a region of interest (ROI) that accommodates 3 × 3 polymer beads. Fluorescence images from this area are shown in Figure 1e on an expanded scale. These were obtained by focusing the UV light for 1 s onto the PS bead P_0 in the centre (dashed purple line) and subsequently probing the fluorescence from all nine PS beads by excitation with VIS light for 29 s (i.e., the total duration of one cycle is 30 s). The two images in Figure 1e have been accumulated during the first 100 ms (left) and the last
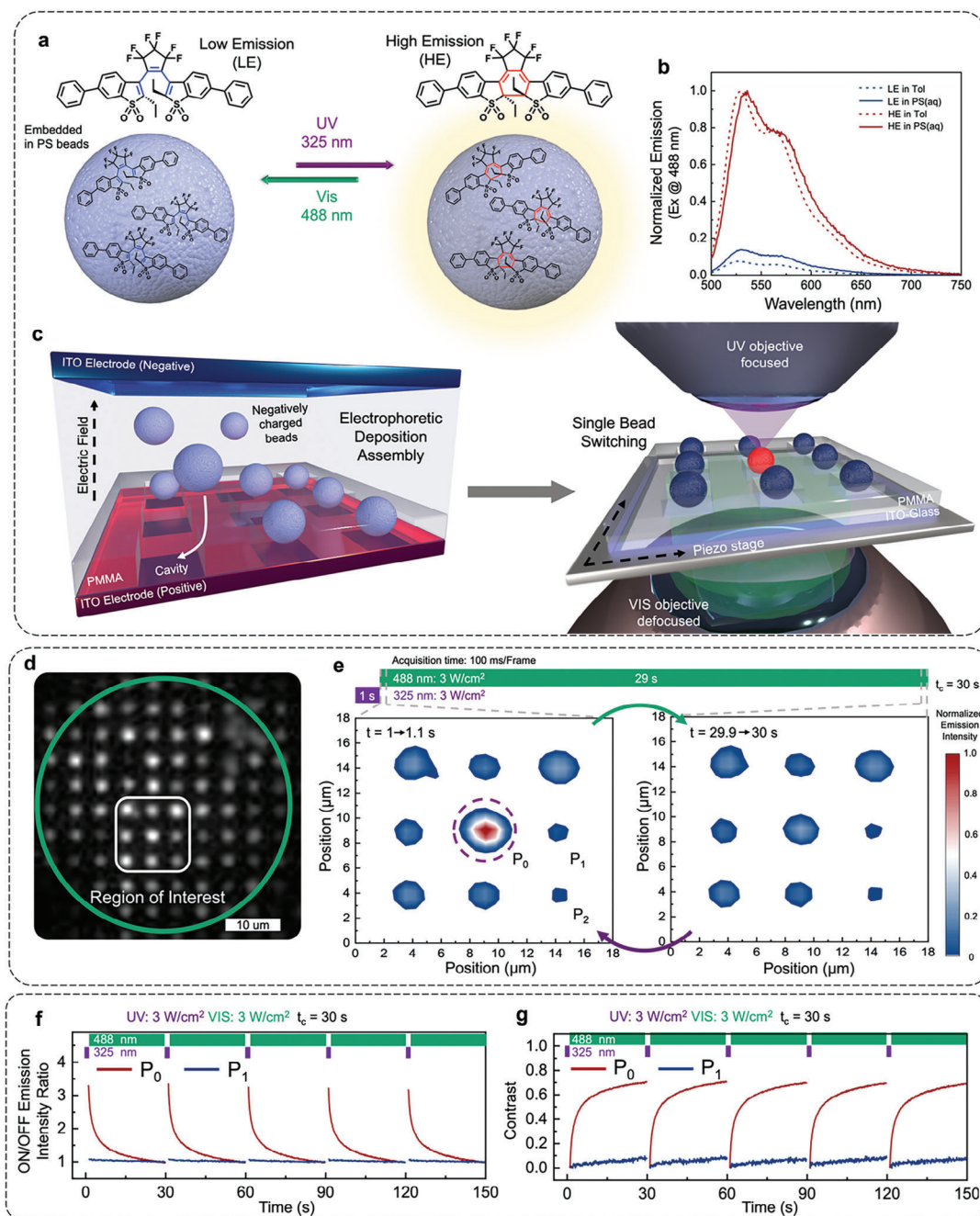
Figure 1. a) Molecular structure of the DAE molecules in the open, low-emissive (LE) state (left), and in the closed, high-emissive (HE) state (right). Bottom: Sketch of polystyrene beads (grey spheres) loaded with DAE molecules. The wavelengths used to induce reversible photoswitching are indicated next to the coloured arrows. b) Emission spectra of DAE in toluene (dashed lines) and polystyrene (full lines) in the LE (blue lines) and HE (red lines) states. The excitation wavelength was 488 nm, and the HE spectra have been normalized. The intensity of the LE spectrum is shown relative to the corresponding HE spectrum. c) Left: Schematic sketch of a sample cell for STEPD. The cell consists of a PMMA substrate (PMMA thickness 50 nm) with predefined cavities (500 nm x 500 nm) prepared with electron beam lithography and is placed between positively and negatively charged ITO electrodes. Right: Sketch of the optical experiment exposing the beads to UV (from the top) and VIS (from the bottom) radiation via two microscope objectives. While the VIS light illuminates a larger area of the sample (70 µm in diameter), the UV light is focussed to a spot size of roughly 500 nm in diameter and can be superimposed selectively on individual nanobeads by moving the whole sample with a piezo stage. d) Example of an array of PS nanobeads arranged on a 5 µm × 5 µm grid with the STEPD method. The green line indicates the area that is illuminated by the visible laser at 488 nm, and the white rectangle corresponds to the region of interest (ROI) that is studied further. e) Fluorescence images of the ROI for an optical cycle of 1s illumination at 325 nm (3 W cm^{-2}) and 29s of illumination at 488 nm (3 W cm^{-2}), as indicated by the bars at the top. The images have been acquired at the beginning (left) and the end (right) of the VIS illumination period for bin times of 100 ms. In the left part, the purple dashed line indicates the area that is irradiated with UV light. The fluorescence intensity has been normalized to the HE level and is colour-coded, see bar at the right. f) Response of the normalized emission intensity (left axis) as a function of time for the beads P_0 (red line) and P_1 (grey line) for five consecutive illumination cycles. g) Contrast C(t) for the beads P_0 (red line) and P_1 (grey line) for five consecutive illumination cycles.
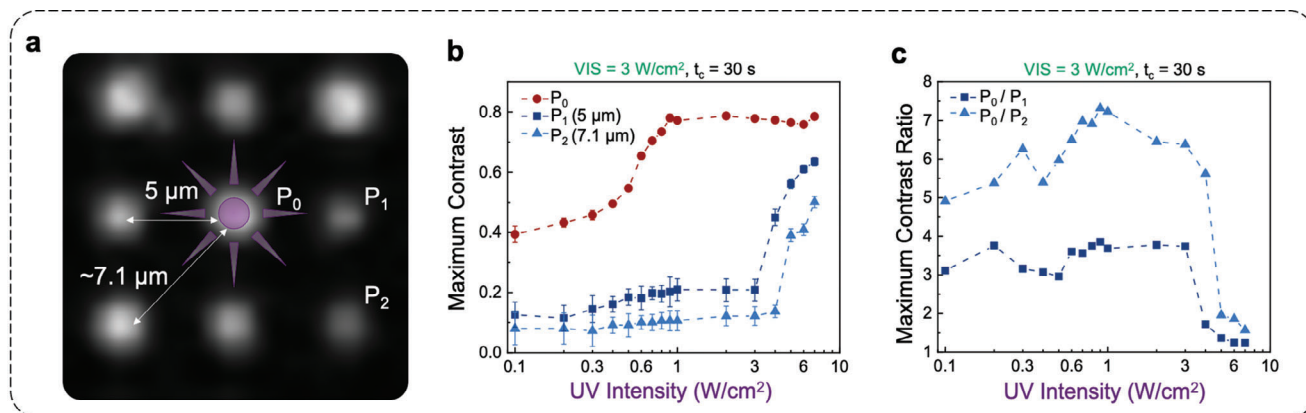
2401029 (3 of 8)

**ADVANCED
SCIENCE NEWS**

www.advancedsciencenews.com

**ADVANCED
OPTICAL
MATERIALS**

www.advopticalmat.de

Figure 2. a) ROI featuring 3×3 DAE-loaded PS beads assembled on a $5\ \mu m \times 5\ \mu m$ grid. P_0 refers to the bead in the centre that is irradiated with UV light (purple dot) prior to probing all beads in the ROI with light in the VIS spectral range. b) Achievable maximum contrast for the beads P_0 (dots), P_1 (squares), and P_2 (triangles) as a function of the UV intensity. The VIS intensity was fixed at $3\ W\ cm^{-2}$, the UV illumination time was 1s, and the cycle time was $t_c = 30\ s$. The numbers in parentheses give the lateral distance between P_0 and P_1 or P_0 and P_2, see part a). c) Ratios of the contrast observed in b) between P_0 and P_1 (triangles), and between P_0 and P_2 (squares) as a function of the UV intensity. In b),c) the lines between the data points serve as a guide for the eye.

100 ms (right) of exposure to VIS light. Only for the bead P_0, whose chromophores have been initialized in the HE state, is a strong fluorescence signal observed upon illumination with VIS light, Figure 1e left, whereas the signal from the other beads remains at the low level. Importantly, as the VIS illumination proceeds, the emission intensity registered from the bead P_0 decays to the LE level on a timescale of several seconds, Figure 1e right. This is compared more quantitatively in Figure 1f for P_0 and one of its nearest neighbouring beads, P_1. The figure shows the normalized emission intensity of these beads for five consecutive UV–vis illumination cycles of 30s duration each. The high degree of reproducibility of the five cycles illustrates the reversibility of the switching process. Taking another point of view, this can be interpreted as a repetition of purely optical write-read-erase cycles. The UV light writes a piece of information into the nanobead that can be read out by fluorescence upon VIS excitation. Prolonged VIS excitation erases this information and clears the bead for a new writing cycle. In order to quantify this optical cycle more precisely, we define the contrast as a function of time as

$$C\ (t) = \frac{I_{max} - I(t)}{I_{max}} = 1 - \frac{I(t)}{I_{max}} \qquad (1)$$

where I_{max} refers to the emission intensity that is obtained at the beginning of the 488 nm illumination period, and $I(t)$ refers to the intensity at time t during the 488 nm illumination period. Since the VIS radiation also converts the DAE molecules to the LE state, $I(t)$ decreases as a function of time, and the maximum contrast between the HE and LE levels is obtained for long 488 nm illumination times. In other words, erasing the information from the previous writing cycle is more complete, the longer the bead is exposed to VIS light. For the beads, P_0 (black line) and P_1 (grey line) the temporal development of the contrast is compared in Figure 1g. For P_0 it shows a steep rise from 0 to 0.5 within a few seconds at the beginning of the 488 nm illumination time and saturates at longer times at ≈ 0.7. For P_1 this parameter shows

only a small change as a function of time from 0 to ≈ 0.1 after 30 s.

2.3. Elucidating Parameters for Optimum Performance

Obviously, the contrast that can be achieved for a particular bead is a function of the illumination intensities of the two conversion beams and the duration of the cycle time. For optical writing/reading/erasing information it is therefore important to find the best combination of these parameters to achieve the largest discriminatory power between the signals. Yet, before this is done, we first address the issue of crosstalk between neighbouring beads. In **Figure 2a**, the ROI of Figure 1d is shown on an enlarged scale specifying the spatial separations between nearest-neighbour beads (5 μm) and next-nearest-neighbour beads (7.1 μm). As before, only the PS bead in the centre, P_0, is irradiated with UV light, converting the incorporated DAE molecules to the closed (HE) conformation.

For a fixed VIS excitation intensity of $3\ W\ cm^{-2}$, Figure 2b shows the maximum contrast as a function of the UV excitation intensity for the bead P_0, one of its nearest neighbours, P_1, and one of its next-nearest neighbours, P_2. For the beads P_1 and P_2 whose chromophores have not been converted to the HE state, the contrast remains almost constant at C = 0.1 up to an excitation intensity of $3\ W\ cm^{-2}$. For excitation intensities above this value, the contrast for these beads rises to about 0.6. This rise is presumably caused by the scattering of the UV radiation toward the beads that are not within the UV focus, resulting in the conversion of some of the DAE molecules to the HE state. This is in contrast to the findings for P_0, whose molecules were initialized to the HE state. For this bead, the contrast already begins to increase at 0.4 for low UV excitation intensities and shows a significant rise to 0.75 at about1 $W\ cm^{-2}$. Dividing the observed contrasts of P_0 and P_1 (P_2) yields the contrast ratios shown in Figure 2c. This reveals ratios above 5 (P_0/P_1) and above 3 (P_0/P_2)
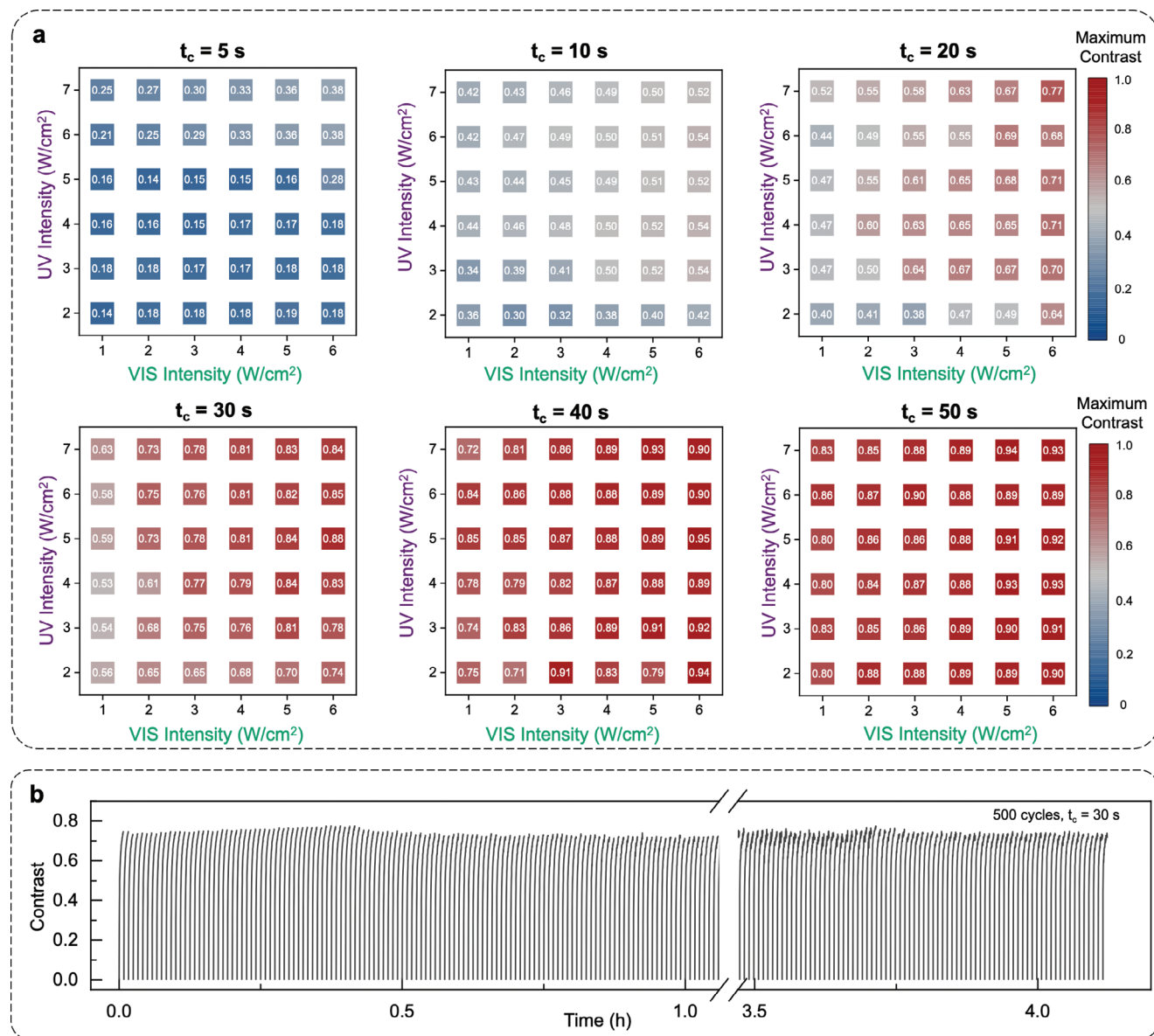
2401029 (4 of 8)

Figure 3. a) Maximum achievable contrast as a function of UV and VIS intensities for cycle times of 5, 10, 20, 30, 40, and 50 s, from top left to bottom right. The contrast values are colour-coded (bar at the right) and given by the numbers in the intensity matrices. b) Contrast as a function of the cycle time for 500 consecutive cycles of 30s each. The total experimental time covers more than 4 h.

for UV excitation intensities below 3 W cm^{-2}, which then both drop to ≈1 for higher UV intensities. Hence, the system exhibits very strong discriminatory power between the HE and LE levels, and at the same time low cross-talk for UV intensities between 1 and 3 W cm^{-2}.

Finally, in order to identify the optimum operational parameters and also to give an overview of photonic unit switching performance, all combinations of excitation intensities ranging from 1 to 6 W cm^{-2} for the VIS and 2–7 W cm^{-2} for the UV (both in increments of 1 W cm^{-2}) have been tested for cycle times t_c of 5, 10, 20, 30, 40, and 50 s. This yields in total six 6 × 6 intensity matrices for the maximum contrast and these are shown in **Figure 3a**. For nearly all applied intensities the contrast rises monotonically as a function of the cycle time because the longer the VIS illumi-

nation time, the greater the number of DAE molecules that are converted back to the LE state. For VIS intensities between 3 and 6 W cm^{-2} the observable contrast does not depend much on the VIS intensity, and the largest growth of the contrast is observed during the first 30 s (from about 0.2 to about 0.8), followed by a further minor increase to about 0.9 after 50 s. For the shortest cycle time of 5 s, it turns out that the maximum achievable contrast is generally poor. For all combinations of excitation intensities, it does not exceed a value of 0.4, and even values above 0.3 can only be achieved at the highest excitation intensities, which are problematic with respect to cross-talk, see above. This reflects the fact that the VIS illumination time of 4 s (not to be confused with the cycle time t_c which includes also 1s of UV illumination) is not long enough to convert a sufficient fraction of DAE molecules
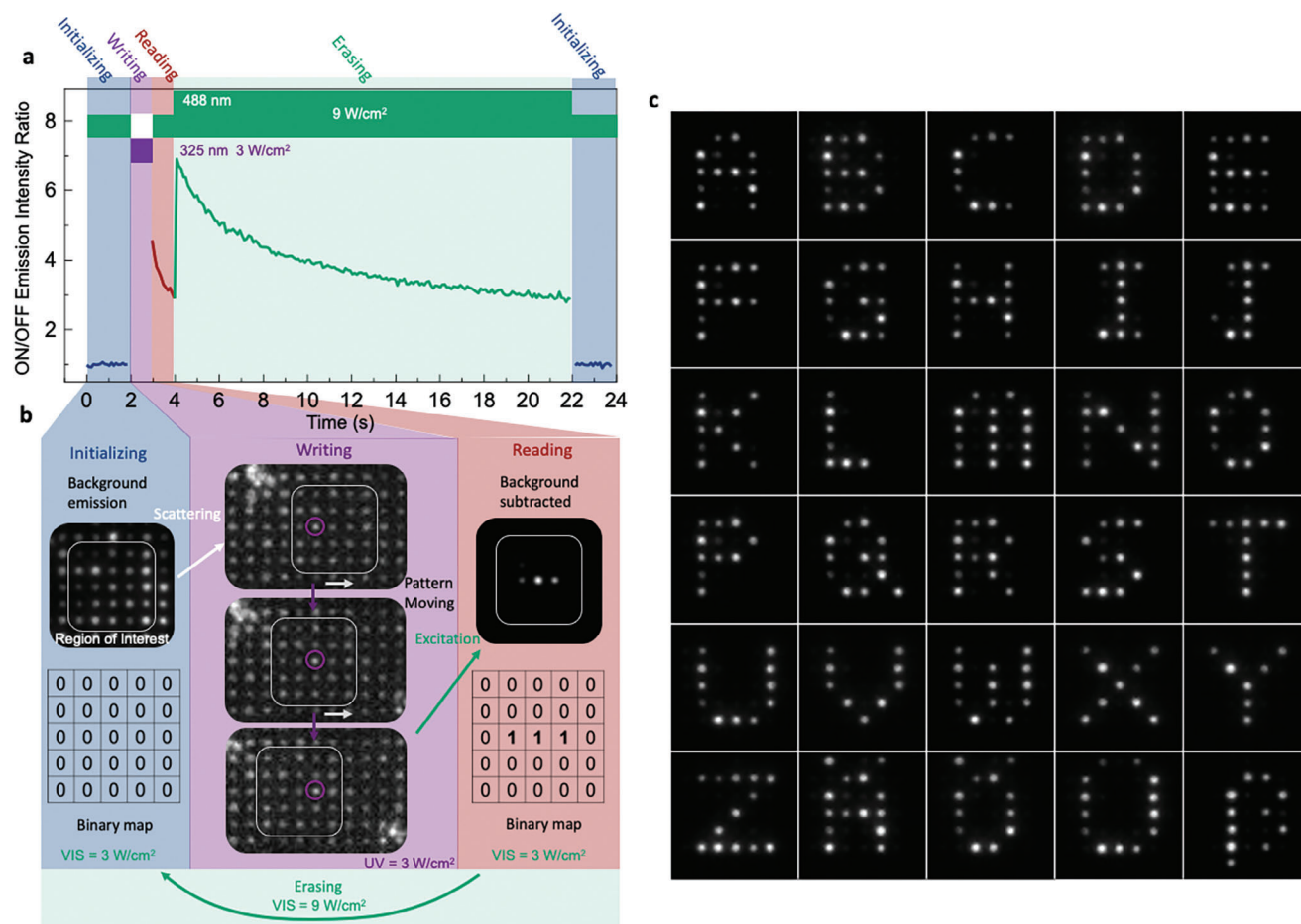
Figure 4. a) Timing sequence for initialization (blue, VIS, 2 s, 3 W cm^{-2}), writing (purple, UV, 1 s, 3 W cm^{-2}), read-out (red, VIS, 1 s, 3 W cm^{-2}), and erasure (green, VIS, 18 s, 9 W cm^{-2}). b) Sample area (ROI) of 5 × 5 DAE loaded PS beads illustrating the initialization (blue, left), writing (purple, centre), read-out (red right), and erasure (green bottom) processes. For writing, the array of PS beads can be moved relative to the focal spot of the UV light, which allows the conversion of the DAE molecules in several beads, one at a time for 1 s, to the HE level. For read-out the sample is probed with VIS light and the fluorescence signal is accumulated during the first 100 ms of the read-out period. Only those beads whose chromophores have been converted to the HE level show a fluorescence signal above background. The corresponding binary output maps are shown as well. c) For illustration the letters of the alphabet have been written consecutively, one after the other, onto the same area of the sample.

back to the LE state. Larger maximum contrasts can be obtained for higher intensities and longer cycle times. For example, for the highest UV and VIS intensities and 50s cycle time, we find C = 0.93.

Given that the UV intensity should not exceed 3 W cm^{-2} to diminish cross-talk, and that an increase in the cycle time from 30 to 50 s yields only a moderate increase in the maximum contrast, we have used a cycle time of $t_c = 30$ s and excitation intensities of 3 W cm^{-2} for both wavelengths to conduct further experiments. This choice is a good compromise between high contrast, suppression of cross-talk, and the duration of the experiment. For this setting of the parameters, Figure 3b shows the contrasts C(t) for 500 consecutive illumination cycles. For all individual cycles, the maximum contrast exceeds 0.7 and does not show any degradation during the more than 4 h of total illumination time, confirming the high photostability of these novel, chemical switching systems.

The results shown so far demonstrate that the DAE-loaded PS beads within the array can be addressed selectively for pho-

tochromic switching. Hence, information can be encoded into the pattern by moving the beads selectively, one by one, into the UV focus, Figure 1c right.

2.4. Reversible Write–Read–Erase Cycling

With the characterization shown above at hand, we now have the ingredients to demonstrate purely optical, write-read-erase cycles on micro-patterned surfaces. The standard procedure applied is as follows (see **Figure 4a,b**): 1) Initialization: Because the DAE molecules in the LE state give rise to a low fluorescence signal, the sample area of interest is illuminated for 2 s with VIS light at 3 W cm^{-2} to convert any equilibrium mixture of LE and HE isomers to LE form so that a standardized LE background can be determined. 2) Writing: With the aid of a piezo stage a PS bead is moved into the focus of the UV light and irradiated for 1 s (3 W cm^{-2}). This converts the DAE molecules of this particular bead into the HE state. Then the next bead is selected and brought

for 1 s into the UV focus by moving the piezostage, (see Figure 4b centre). This is repeated for as many PS beads as are required to encode specific information into the microarray of PS beads (see Movie S1, Supporting Information). At the end of this procedure, the array contains a selected group of PS beads that contain DAE molecules "sleeping" in the HE state. 3) Read-Out: The whole sample area is illuminated for 1 s with VIS light (3 W cm^{-2}). This results in a strong fluorescence from those PS beads whose DAE molecules had been converted into the HE state (Figure 4b right). 4) Erasure: The sample is illuminated for 18 s with VIS light at an intensity of 9 W cm^{-2}. The increased VIS intensity is applied in order to accelerate the recovery of the DAE molecules from the HE back to the LE state. It is important to note that the VIS intensity applied during Initialization (step 1) and Read-Out (step 3) have to be identical in order to correctly take the background into account. As a simple proof of the efficacy of this optical encoding system, the letters of the alphabet have been written consecutively onto the *same* 5 × 5 PS array of beads in the sample, see Figure 4c.

3. Discussion

Over the last few decades much attention has been given to the demonstration of the function of molecular logic circuits.[2,4,39] However, very often, at least some of the transitions between the molecular states were induced using diffusion-limited processes such as enzymatic reactions, pH changes, and/or temperature changes that slow down the speed of operation.[40,41] This has inspired many researchers to investigate the potential of all-optical data processing, i.e., using light as an external stimulus.[3,42] Although the basic functionality of an optical transistor was demonstrated in several benchmark experiments, the systems used featured either low gain,[43,44] were operated at cryogenic temperatures,[43] relied on non-linear, light-matter interactions needing strong electric fields,[45] i.e., very high light intensities, or they consisted of self-assembled DNA nanostructures.[46]

Beyond proof-of-principle experiments, the realization of photonic logic gates, i.e., circuits that run on photons rather than electrons, requires building blocks that allow reversible generation of binary outputs with high discriminatory power. The reversible writing, reading, and erasing of information by optical means was demonstrated.[47] Yet, each individual step took several minutes and the sample was illuminated through a photomask. Alternatively, in[48] confocal illumination techniques were used to write different images within seconds repetitively onto a surface that consisted of a photoswitchable, inorganic-organic hybrid system. However, since logic circuits require concatenation and this in turn requires light from one source to control and manipulate light from another source, precise positioning of the switchable units with respect to each other is crucial. This necessitates actively patterned surfaces for control and spacing of the spatial arrangement of the photoswitchable units. As a first step towards this goal, we have demonstrated that micropatterned arrays of polymer beads loaded with photochromic molecules can be prepared and addressed selectively to inscribe information. We have elucidated the interplay of external stimuli, such as the illumination intensities and illumination times for writing, reading, and erasing of information to achieve the optimum contrast and minimum cross-talk. The functionality of this approach is exemplified by consecutively writing, reading and erasing the letters of the alphabet onto the same 25 polymer beads arranged in a 5 μm × 5 μm matrix, which took only a few seconds per step. Taking advantage of the large variety of derivatives of photochromic DAE molecules, this can be exploited to create variations of the emission wavelengths for particular photonic units. This provides spectral selectivity as a further parameter. Together with modern patterning techniques, this opens a route for the concatenation of several photonic units for accomplishing interconnected photonic logic gates. In summary, these results demonstrate that photochromism can be used to undertake logic functions using photons as signal carriers.

Supporting Information

Supporting Information is available from the Wiley Online Library or from the author.

Conflict of Interest

The authors declare no conflict of interest.

Data Availability Statement

The data that support the findings of this study are available from the corresponding author upon reasonable request.

[1] P. A. de Silva, N. H. Q. Gunaratne, C. P. McCoy, *Nature* **1993**, *364*, 42.

[2] (Ed: A. P. de Silva), *Molecular Logic-Based Computation*, Royal Society of Chemistry, Cambridge **2013**.

[3] U. Pischel, J. Andreasson, D. Gust, V. F. Pais, *Chem. Soc. Rev.* **2013**, *14*, 28.

[4] K. Szacilowski, *Chem. Rev.* **2008**, *108*, 3481.

[5] B. L. Feringa, *Molecular Switches*, Wiley-VCH, Weinheim, Germany **2011**.

[6] (Eds: H. Dürr, H. Bouas-Laurent), *Photochromism: Molecules and Systems*, Elsevier, Amsterdam **2006**.

[7] (Ed: G. H. Brown), *Photochromism*, Wiley, New York **1971**.

[8] W. R. Browne, B. L. Feringa, *Annu. Rev. Phys. Chem.* **2009**, *60*, 407.

[9] M. Irie, *Chem. Rev.* **2000**, *100*, 1685.

[10] J. Boulanger, C. Gueudry, D. Münch, B. Cinquin, P. Paul-Gilloteaux, S. Bardin, C. Guérin, F. Senger, L. Blanchoin, J. Salamero, *Proc. Natl. Acad. Sci. USA* **2014**, *111*, 17164.

[11] M. Barale, M. Escadeillas, G. Taupier, Y. Molard, C. Orione, E. Caytan, R. Métivier, J. Boixel, *J. Phys. Chem. Lett.* **2022**, *13*, 10936.

[12] F. M. Raymo, S. Giordani, *Proc. Natl. Acad. Sci. U. S. A.* **2002**, *99*, 4941.

[13] J. Andréasson, D. Gust, In *Molecular and Supramolecular Information Processing* (Ed.: E. Katz), Wiley-VCH, Weinheim, Germany **2012**, pp. 53.

[14] P. Hong, N.-H. Xie, K. Xiong, J. Liu, M.-Q. Zhu, C. Li, *J. Mater. Chem. A* **2023**, *11*, 5703.

[15] P. Hong, J. Liu, K.-X. Qin, R. Tian, L.-Y. Peng, Y.-S. Su, Z. Gan, X.-X. Yu, L. Ye, M.-Q. Zhu, C. Li, *Angew Chem Int Ed Engl* **2024**, *63*, e202316706.

[16] Q.-F. Li, L. Zhang, M. Shen, J.-T. Wang, L. Jin, Z. Wang, *J. Mater. Chem. C* **2023**, *11*, 12828.

[17] C. Shi, R. Zhu, K. Guo, L. Zhang, Z. Liu, X. Liu, Q. Ai, X. Hu, *Adv. Opt. Mater.* **2023**, *11*, U84.

[18] J. Andreasson, S. D. Straight, G. Kodis, C.-D. Park, M. Hambourger, M. Gervaldo, B. Albinsson, T. A. Moore, A. L. Moore, D. Gust, *J. Am. Chem. Soc.* **2006**, *128*, 16259.

[19] J. Andréasson, U. Pischel, S. D. Straight, T. A. Moore, A. L. Moore, D. Gust, *J. Am. Chem. Soc.* **2011**, *133*, 11641.

[20] M. Bälter, S. Li, J. R. Nilsson, J. Andréasson, U. Pischel, *J. Am. Chem. Soc.* **2013**, *135*, 10230.

[21] G. Naren, S. Li, J. Andréasson, *ChemPhysChem* **2017**, *18*, 1726.

[22] M. F. Budyka, V. M. Li, *ChemPhysChem* **2017**, *18*, 260.

[23] A. T. Hendra, H. Yamagishi, O. Oki, M. Morimoto, M. Irie, Y. Yamamoto, *Adv. Funct. Mater.* **2021**, *31*, 2103685.

[24] H. Y. Hendra, W. Y. Heah, A. D. Malay, K. Numata, Y. Yamamoto, *Adv. Opt. Mater.* **2023**, *11*, 2202563.

[25] M. Irie, M. Morimoto, *B. Chem. Soc. Jpn.* **2018**, *91*, 237.

[26] D. Kim, J. E. Kwon, S. Y. Park, *Adv. Funct. Mater.* **2018**, *28*, 1706213.

[27] Y.-C. Jeong, S. I. Yang, K.-H. Ahn, E. Kim, *Chem Commun (Camb)* **2005**, *19*, 2503.

[28] K. Uno, H. Niikura, M. Morimoto, Y. Ishibashi, H. Miyasaka, M. Irie, *J. Am. Chem. Soc.* **2011**, *133*, 13558.

[29] A. Albert, M. Fried, M. Thelakkat, J. Köhler, *Phys. Chem. Chem. Phys.* **2022**, *24*, 29791.

[30] H. Yamagishi, T. Matsui, Y. Kitayama, Y. Aikyo, L. Tong, J. Kuwabara, T. Kanbara, M. Morimoto, M. Irie, Y. Yamamoto, *Polymers* **2021**, *13*, 269.

[31] J. Maier, M. Pärs, T. Weller, M. Thelakkat, J. Köhler, *Sci. Rep.* **2017**, *7*, 41739.

[32] J. Maier, T. Weller, M. Thelakkat, J. Köhler, *J. Chem. Phys.* **2021**, *155*, 14901.

[33] F. Cichos, C. von Borczyskowski, M. Orrit, *Curr. Opin. Colloid In.* **2007**, *12*, 272.

[34] M. Nirmal, B. O. Dabbousi, M. G. Bawendi, J. J. Macklin, J. K. Trautman, T. D. Harris, L. E. Brus, *Nature* **1996**, *383*, 802.

[35] E. K. L. Yeow, S. M. Melnikov, T. D. M. Bell, F. C. de Schryver, J. Hofkens, *J. Phys. Chem. A* **2006**, *110*, 1726.

[36] M. Lippitz, F. Kulzer, M. Orrit, *ChemPhysChem* **2005**, *6*, 770.

[37] R. Kashihara, M. Morimoto, S. Ito, H. Miyasaka, M. Irie, *J. Am. Chem. Soc.* **2017**, *139*, 16498.

[38] H. Zhang, J. Cadusch, C. Kinnear, T. James, A. Roberts, P. Mulvaney, *ACS Nano* **2018**, *12*, 7529.

[39] S. Zanella, M. A. Hernández-Rodríguez, R. A. S. Ferreira, C. D. S. Brites, *Chem Commun (Camb)* **2023**, *59*, 7863.

[40] T. Gupta, M. E. van der Boom, *Angew. Chem., Int. Ed.* **2008**, *47*, 5322.

[41] E. Katz, V. Privman, *Chem. Soc. Rev.* **2010**, *39*, 1835.

[42] J. Andreasson, U. Pischel, *Chem. Soc. Rev.* **2015**, *44*, 1053.

[43] J. Hwang, M. Pototschnig, R. Lettow, G. Zumofen, A. Renn, S. Götzinger, V. Sandoghdar, *Nature* **2009**, *460*, 76.

[44] M. Pärs, C. C. Hofmann, K. Willinger, P. Bauer, M. Thelakkat, J. Köhler, *Angew. Chem., Int. Ed.* **2011**, *50*, 11405.

[45] D. E. Chang, A. S. Sørensen, E. A. Demler, M. D. Lukin, *Nat. Phys.* **2007**, *3*, 807.

[46] C. D. LaBoda, A. R. Lebeck, C. L. Dwyer, *Nano Lett.* **2017**, *17*, 3775.

[47] N.-H. Xie, C. Fan, H. Ye, K. Xiong, C. Li, M.-Q. Zhu, *ACS Appl. Mater. Interfaces* **2019**, *11*, 23750.

[48] C. Lee, E. Z. Xu, K. W. C. Kwock, A. Teitelboim, Y. Liu, H. S. Park, B. Ursprung, M. E. Ziffer, Y. Karube, N. Fardian-Melamed, C. C. S. Pedroso, J. Kim, S. D. Pritzl, S. H. Nam, T. Lohmueller, J. S. Owen, P. Ercius, Y. D. Suh, B. E. Cohen, E. M. Chan, P. J. Schuck, *Nature* **2023**, *618*, 951.